Draft version December 2, 2023
Typeset using LaTeX **modern** style in AASTeX631

`nuance`: Detection of planetary transits in the presence of correlated noise

Lionel J. Garcia,[1] Daniel Foreman-Mackey,[1] Dax L. Feliz,
Catriona A. Murray, and Francisco J. Pozuelos

[1] *Center for Computational Astrophysics, Flatiron Institute, New York, NY, USA*

ABSTRACT

We present *nuance*, an algorithm to search for planetary transits in light curves featuring correlated noise, such as instrumental signals and stellar photometric variability. To deal with these nuisance signals, a common approach consists in cleaning a light curve from correlated noise before searching for transits. However, we show that this approach, based on the prior assumption that transits are not present, strongly degrades their signals, up to the point of no detection. As this degradation depends on the correlated noise characteristics, we explore the parameter space for which transits are altered, and quantify this effect on a wide variety of cases. We show that *nuance* outperforms the detection capabilities of commonly used transit search algorithms, especially for light curves featuring correlated noise with an amplitude three times greater than the searched transit depth. We perform our tests by injecting transits on synthetic light curves, and on known TESS candidates light curves to assess the performance of our algorithm on realistic multi-planetary systems datasets. Beyond its detection efficiency, we make *nuance* tractable, `todo` times faster than current alternatives based on brute force detrending, and available as a well documented open-source Python package[a)].

INTRODUCTION

Transiting exoplanets are keystone objects for the field of exoplanetary science, but detecting transits in light curves featuring stellar variability and instrumental signals remains a challenge (Pont et al. 2006; Howell et al. 2016). For this reason, known transiting exoplanets tend to be found around quieter stars, or belong to the population of close-in giants whose transit signals dominate over stellar rotational variability (Simpson et al. 2023). However, discovering transiting exoplanets around active stars holds few promises. First, as younger stars are more active[1] (Skumanich

Corresponding author: Lionel J. Garcia
lgarcia@flatironinstitute.org

[a)] https://github.com/lgrcia/nuance

[1] approximately down to spectral type MV ()

1972), being able to detect planets transiting active stars will favor the discovery of young planetary systems (e.g. Newton et al. 2022). Second, as stellar variability may originate from surface active regions (such as starpots), the increased discovery of occulting companions will increase our chances to map the photosphere of active stars (e.g. Morris et al. 2017), benefiting both the study of stellar atmospheres and the concerning impact of their non-uniformity on planetary atmosphere retrievals (Rackham et al. 2018). Overall, enabling the detection of transits in light curves with high levels of correlated noises will greatly benefit the study of terrestrial exoplanets around late M-dwarfs, usually observed at lower SNR and more likely to display photometric variability (e.g. Murray et al. 2020).

Commonly used transit-search algorithms, such as the Box-Least-Square algorithm (BLS, Kovács et al. 2002) are capable of detecting transits in light curves containing only transit signals and white noise. Using this method, the simplest way to detect transits in a light curve featuring correlated noise (either astrophysical or instrumental), is to first clean it from nuisance signals before performing the search. This strategy is widely adopted by the community, both using physically-motivated systematic models like Luger et al. (2016, 2018), or filtering techniques (Jenkins et al. 2010, Hippke et al. 2019). However, when correlated noise starts resembling transits, this cleaning step (often referred to as *detrending*) is believed to degrade their detectability (see subsection 4.3 of Hippke et al. 2019). In this case, the only alternative to search for transits is to perform a full-fledged modeling of the light curve, including both transits and correlated noise, and to compute the likelihood of the data to the transit model on a wide parameter space (an approach largely avoided due to its intractable nature). Nonetheless, Kovács et al. (2016) ask: *Periodic transit and variability search with simultaneous systematics filtering: Is it worth it?*. The latter study explores a handful of cases and generally discards the benefit of using a full-fledged approach. However, it does not explore the light-curves characteristics for which such a complete modeling becomes necessary.

In this paper, we explore the light curve characteristics for which a full-fledge transit search is necessary, and we present *nuance*[2], a method to search for transit signals while modeling correlated noises in a tractable way. In section 1, we describe the effect of correlated noise on transit light curves and the effect of its detrending on planetary signals detectability. In section 2, we present *nuance*. In section 3, we test the performance of *nuance* on a wide variety of cases, and compare it to commonly used transit search algorithms. Finally, in section 4, we discuss the results and the limitations of *nuance*, and we conclude in **??**.

[2] Throughout the paper, *nuance* typeseted in italics reference to the method, while nuance in sans-serif reference to its implementation.

1. THE ISSUE

A strong assumption when using BLS-based algorithms is that the searched dataset only contains transit signals and white noise. Hence, two sources of correlated noise particularly justify the need for a detrending step before searching for transits: instrumental signals (such as those induced by telescope pointing errors) and astrophysical signals (such as stellar variability induced by pulsations or starspots). In this section, we qualitatively study the effect of correlated noise and its detrending on transits detectability.

1.1. *Transit detectability*

One way to study the detectability of a unique transit signal is to compute its signal-to-noise-ratio (SNR, Pont et al. 2006, Equation 12):

$$SNR = \frac{\Delta}{\sqrt{\frac{\sigma_w^2}{n} + \frac{\sigma_c^2}{N_{tr}}}} \tag{1}$$

where Δ is the relative transit depth, n is the number of points within transit, N_{tr} the number of transits ($N_{tr} = 1$ here), and σ_w^2 and σ_c^2 are the white and correlated noise variances. Figure 1 shows this metric computed for a unique transit observed in the absence (grey) and presence (red) of correlated noise.

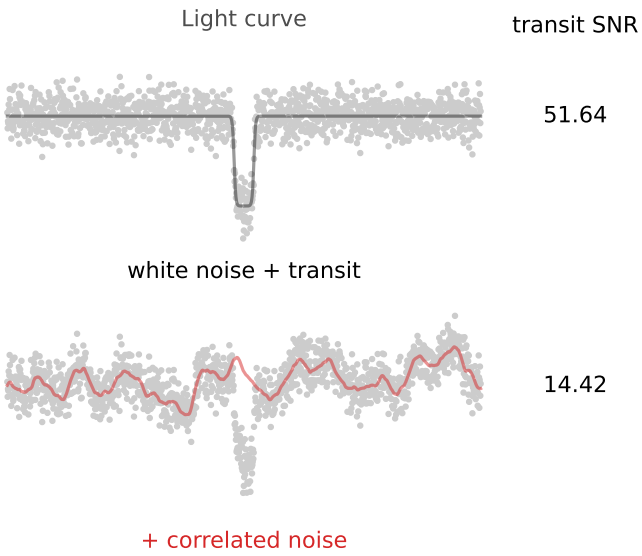

Figure 1. Illustration of the effect of correlated noise on a single transit SNR. A 1-hour transit signal of depth 1% is generated on top of white noise (variance of 0.0015^2) as part of a 24-hours observation with an exposure time of 1 minute (top). Then, in the bottom plot, correlated noise is added, generated using a Gaussian Process with a Matèrn-32 kernel of scale 1 hour and sigma of 0.2%. The SNR on the right of each light curve is computed using Equation 1. Models used to simulate these data are provided in Appendix A.

As illustrated in Figure 1, the presence of correlated noise strongly decreases the transit signal SNR, which would ultimately limit its detectability.

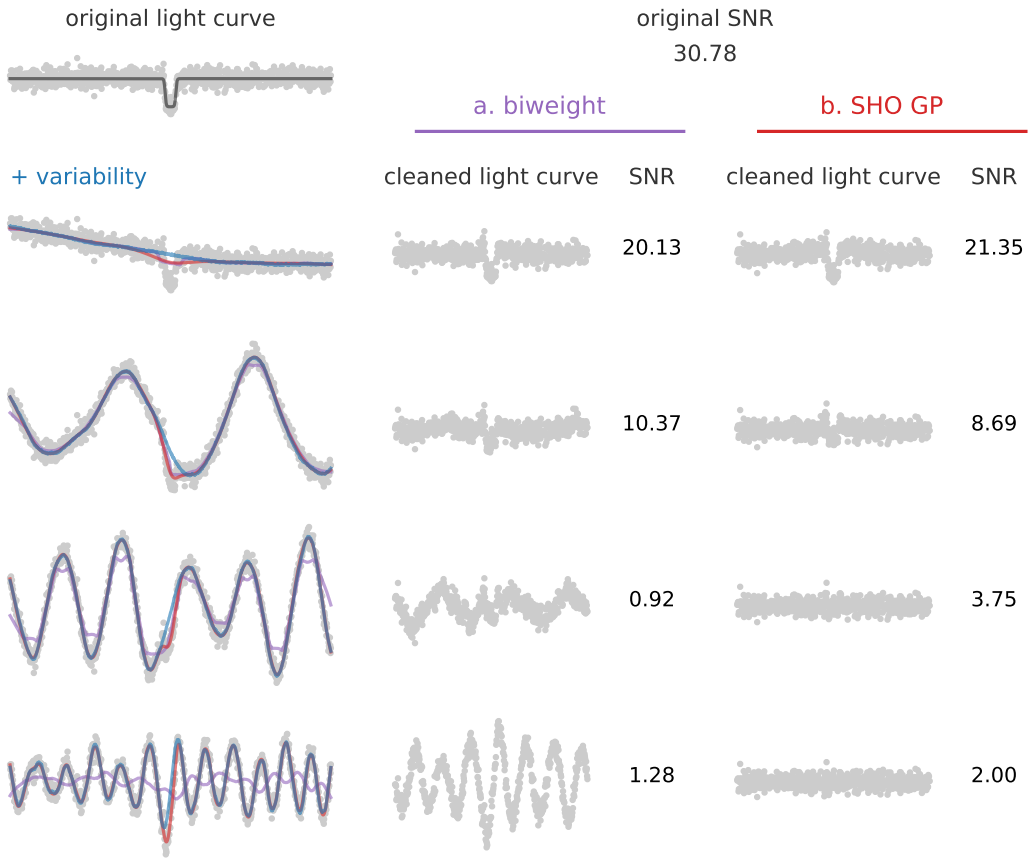

Figure 2. (Top left) Simulated observation spanning 3 days, including a transit signal with a depth of 0.8%, duration of 0.1 day, and measurement error of 1.5% (using the model from Protopapas et al. (2005) described in subsection A.1). (Left) Correlated noise in the form of stellar variability with different timescales and amplitudes added to the unique transit signal. This signal is then reconstructed using (in purple) Tukey's bi-weight filter (Hippke et al. 2019) with an optimal window size of three times the transit duration, and (in red) a Gaussian Process with the same kernel used to simulate the data. In each case the variability is reconstructed, subtracted, and the transit SNR computed using Equation 1 with the transit depth estimated as the minimum in-transit flux.

The presence of instrumental correlated noise motivated the development of systematics detrending algorithms, such as the Trend Filtering Algorithm (TFA, Kovács et al. 2005, in its primary use case), SysRem (Tamuz et al. 2005) or Pixel Level Decorrelation (PLD, Deming et al. 2015; see also Everest from Luger et al. 2016, 2018). Most of these methods rely on the shared nature of instrumental signals among light-curves (or neighboring pixels) such that the correction applied should not degrade the transit signal and can be modeled using contemporaneous measurements (like detector's temperature, pointing error, sky background or airmass time series). In opposition, stellar variability and other astrophysical signals cannot be correlated

with simultaneous measurements. This gave rise to several treatments in order to reconstruct and detrend stellar variability. One of them is physically-motivated and makes use of Gaussian processes (e.g. Aigrain et al. 2016), another is empirical and makes use of filtering algorithms (Jenkins et al. 2010, Hippke et al. 2019).

In Figure 2, we simulate a transit signal on top of which we add photometric stellar variability with different amplitudes and timescales, sampled from a Gaussian Process with an SHO kernel described in subsection A.3. For each light curve, we reconstruct and detrend stellar variability in two ways: one using the widely-adopted Tukey's bi-weight filter, presented in Mosteller & Tukey (1977) and using the implementation from wõtan[3] (Hippke et al. 2019); the other using the same Gaussian Process from which the data has been sampled. We then estimate the resulting transit depth and compute the remaining transit SNR using Equation 1. Figure 2 clearly shows the effect of both detrending techniques on transits SNR, and intuitively suggests that the degradation is strongly dependant on the correlated noise characteristics encountered.

In order to explore the parameter space for which detrending is the most problematic, we employ the method previously described to simulate 10 000 light curves containing a transit signal and correlated noise in the form of stellar variability. For each light curve, we reconstruct the variability signal and detrend it using an optimal bi-weight filter before estimating the remaining transit SNR. For convenience, the simulated light curves share a common transit added on top of white noise, and a variability signal only defined by two parameters: τ, the relative timescale of the variability with respect to the transit duration; and δ, the relative amplitude of the variability against transit depth, corresponding to an SHO kernel with hyperparameters chosen as:

$$\omega = \frac{\pi}{\tau D}, \quad \sigma = \delta\frac{\Delta}{2} \quad \text{and} \quad Q = 10, \tag{2}$$

with $\Delta = 1\%$ and $D = 0.04$ days, the depth and duration of the simulated transit. For $\tau = 1$ and $\delta = 1$, the expressions of ω and σ given in Equation 2 correspond to a variability signal with a period half that of the transit duration, and a standard deviation two times that of the transit depth, i.e. strongly resembling the simulated transit signal.

Figure 3 shows that it exists an entire region of the (τ, δ) parameter space for which the bi-weight detrending degrades transit SNR to the point of no detection ($SNR < 6$). Hence, bi-weight filter detrending makes transit-search blind to many systems. While this study should be extended to other detrending techniques, it highlights the need for a more informed transit search algorithm able to deal with correlated noise.

[3] https://github.com/hippke/wotan

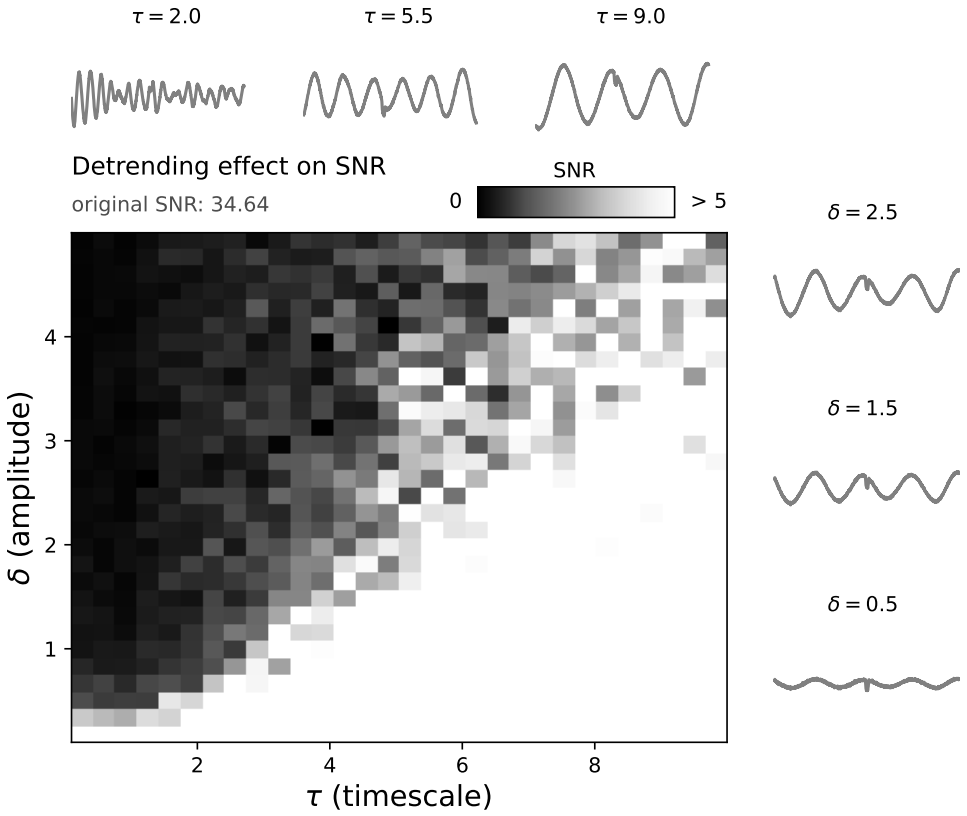

Figure 3. SNR of a unique transit after detrending light curves using an optimal bi-weight filter. All light curves correspond to a 2.8 days observation with a cadence of 2 minutes, and contain a unique transit of duration 1 hour and a depth of 1%, added on top of white noise with a standard deviation of 0.5% plus stellar variability. Light curves at the top and right side of the central plot are shown with their corresponding τ and δ values. The amplitude of the variability increases with δ and the timescale of the variability increases with τ.

2. NUANCE

nuance is an algorithm capable of searching for planetary transits in light curves containing correlated noise, such as instrumental signals and photometric stellar variability.

Let assume that the flux f of a star is observed and arranged in the vector $\boldsymbol{f}$ of size N, associated to the vector of times $\boldsymbol{t}$. This flux, shown in Figure 4, contains instrumental signals, stellar variability and a periodic transit signal that we wish to uncover. We assume that a set of M observed measurements (such as the position of the star on the detector or the sky background) taken at the same time as the flux can be treated as explanatory variables for $\boldsymbol{f}$. These measurements constitute the columns of the $(N \times M)$ *design matrix* $\boldsymbol{X}$.

Ideally, we would detect the periodic transit signal in this flux by sampling the posterior likelihood of this data to a full-fledge model including stellar variability (more generally correlated noise), instrumental systematic signals (modeled with explanatory variables or treated as correlate noise), and a periodic transit signal of period P, epoch T_0, duration D and depth Δ. We would then reduce the posterior likelihood to $p(\boldsymbol{f}|P)$, its marginalized version over all parameters except the period P, producing a transit search periodogram $\mathcal{Q}(P)$. However, this approach has two issues: It is highly intractable, and it may lead to multimodal distributions that are hard to interpret.

Given a period P, we instead want to compute the likelihood of a periodic transit signal at the maximum likelihood parameters $\hat{T}_0$, $\hat{D}$ and $\hat{\Delta}$, i.e the periodogram

$$\mathcal{Q}(P) = p(\boldsymbol{f}|P, \hat{T}_0, \hat{D}, \hat{\Delta}) \tag{3}$$

This is done by adopting the strategy of Foreman-Mackey et al. (2015), and separate the transit search into two components: the *linear search* and the periodic search. During the *linear search*, the likelihood of a single non-periodic transit is computed for a grid of epochs, durations and depths. Then, the periodic search consists in combining these likelihoods to compute the likelihood of the data given a periodic transit signal for a range of periods. These combined likelihoods yield a transit-search periodogram on which the periodic transit detection is based. nuance differs from Foreman-Mackey et al. (2015) and other existing transit search algorithms as it models the covariance of the light curve with a Gaussian Process, accounting for correlated noise (especially in the form of stellar variability) while keeping the model linear and tractable. This way, nuance searches for transits while, at the same time, modeling correlated noise, avoiding the detrending step that degrades transit signals SNR.

We note that the approach employed by nuance (using the two steps proposed by Foreman-Mackey et al. 2015), shares similarities with the approach of Jenkins et al. (2010), where a single event statistic is computed and combined into a multiple event statistics.

2.1. *The linear search*

During the *linear search*, the goal is to compute the likelihood $p(\boldsymbol{f}|T, D, \Delta)$ of the data given a single non-periodic transit signal of epoch T, duration D and depth Δ, for a grid of epochs, durations and depths.

To account for correlated noise, the light curve f is modeled as being drawn from a Gaussian Process, like the simulated light curves used in section 1, such that

$$\boldsymbol{f} \sim \mathcal{N}(\boldsymbol{X}\boldsymbol{w}, \boldsymbol{\Sigma}),$$

with mean $\boldsymbol{X}\boldsymbol{w}$ (i.e. a linear model of the M explanatory variables with coefficients $\boldsymbol{w}$) and covariance $\boldsymbol{\Sigma}$. To account for the presence of a single non-periodic transit of epoch T and duration D, this signal is computed and appended as the last column of the design matrix $\boldsymbol{X}$, using the simple transit model from Protopapas et al. (2005) with a unitary depth (Equation A1). This way, the transit signal is part of the linear model and its depth Δ can be solved linearly. Under this assumption, the log-likelihood of the data given a single non-periodic transit is (Rasmussen & Williams 2005)

$$\ln p(\boldsymbol{f}|I) = -\frac{1}{2}(\boldsymbol{f} - \boldsymbol{X}\boldsymbol{w})^T\boldsymbol{\Sigma}^{-1}(\boldsymbol{f} - \boldsymbol{X}\boldsymbol{w}) - \frac{1}{2}\ln|\boldsymbol{\Sigma}| - \frac{N}{2}\ln 2\pi, \tag{4}$$

where the parameters vector $\boldsymbol{w}$ and their errors $\boldsymbol{\sigma}$ are computed using the generalized least-square solution

$$\boldsymbol{w} = (\boldsymbol{X}^T\boldsymbol{\Sigma}^{-1}\boldsymbol{X})^{-1}\boldsymbol{X}^T\boldsymbol{\Sigma}^{-1}\boldsymbol{f} \quad \text{and} \quad \boldsymbol{\sigma} = (\boldsymbol{X}^T\boldsymbol{\Sigma}^{-1}\boldsymbol{X})^{-1}, \tag{5}$$

with $\boldsymbol{\Sigma}$ the covariance matrix modeled using the Gaussian Process. Hence, $\ln p(\boldsymbol{f}|I)$ can be computed on a grid of epochs and durations, the transit depth being linearly solved for any (T, D). In this equation. This *linear search* leads to the set of likelihoods

$$\{\ln \mathcal{L}_{i,j}\}_{i,j} = \{\ln p(\boldsymbol{f}|T_i, D_j, \Delta_{i,j})\}_{i,j},$$

were $\Delta_{i,j}$ is the depth linearly solved for a given (T_i, D_j)[4]. Figure 4 shows this likelihood grid computed for a simulated dataset, using the same Gaussian Process and design matrix $\boldsymbol{X}$ used to simulate the data.

[4] The expression of $\{\ln \mathcal{L}_{i,j}\}_{i,j}$ omits the vector $\boldsymbol{w}_{i,j}$ (except its last value $\Delta_{i,j}$) as it is also linearly solved for any given value of (T_i, D_j) and irrelevant in what follows.

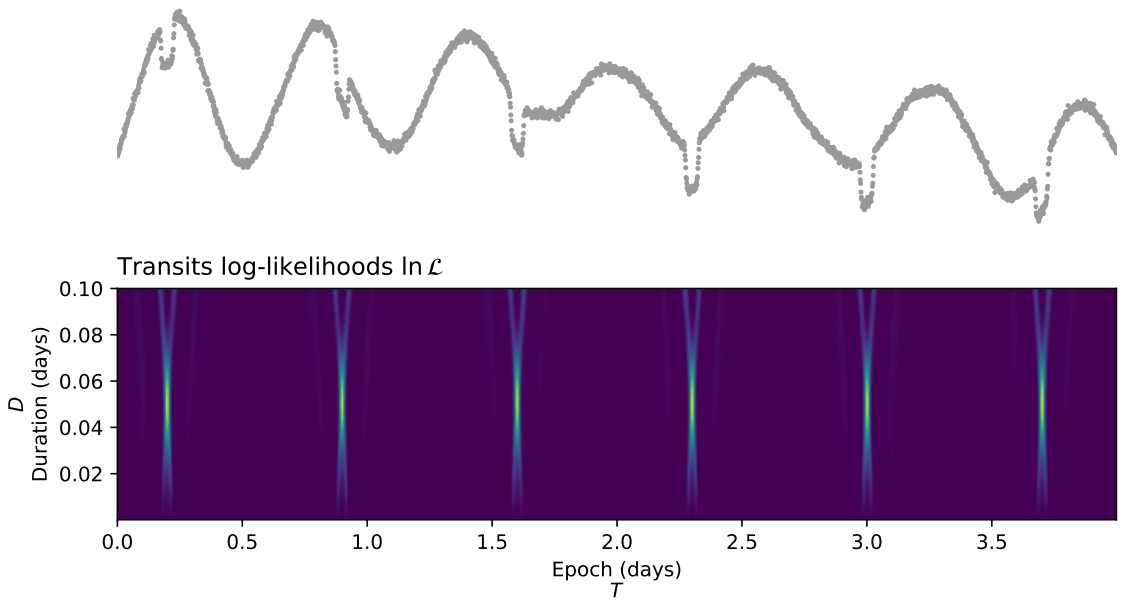

Figure 4. Principle and output of the *linear search*. The simulated dataset (top) corresponds to the one shown and described in Figure 15. First, a set of durations and depths $\{ T_i, D_j \}_{i,j}$ is generated. For each pair of indices (i, j), the likelihood $\ln p(\boldsymbol{f}|T_i, D_j, \Delta_{i,j})$ is computed using the parameters from Equation 5 and the expression of Equation 4. This process yields the grid of log-likelihoods $\ln \mathcal{L}$ (bottom plot), as well as the $\{ \Delta_{i,j}, \sigma_{i,j} \}_{i,j}$ transit depths and errors inferred linearly using Equation 5.

To prepare for the next step, the corresponding depths $\Delta_{i,j}$ linearly solved for any (T_i, D_j) are stored, as well as their associated uncertainties $\sigma_{i,j}$, corresponding to

$$\Delta_{i,j} = \boldsymbol{w}_M \quad \text{and} \quad \sigma_{i,j} = \boldsymbol{\sigma}_{MM},$$

M denoting the index of the last column of the design matrix $\boldsymbol{X}$, where the transit signal is contained.

2.2. *The periodic search*

We then need to combine the likelihoods computed from the *linear search* to obtain

$$p(\boldsymbol{f}|P, T_0, D, \Delta),$$

i.e. the probability of a periodic transit of period P, epoch T_0, duration D and depth Δ given the data $\boldsymbol{f}$. For a given transit duration D, any combination of (P, T_0) leads to K transits, for which it is tempting to write

$$p(\boldsymbol{f}|P, T_0, D, \Delta) = \prod_k^K p(\boldsymbol{f}|T_k, D, \Delta_k), \tag{6}$$

where $\{ T_k \}_k$ are the epochs matching (T_0, P) and $\{ \Delta_k \}_k$ the corresponding depths. So that

$$\ln p(\boldsymbol{f}|P, T_0, D, \Delta) = \sum_k^K \ln \mathcal{L}_k.$$

This is the joint likelihood of transits belonging to the same periodic signal but with varying depths $\{\,\Delta_k\,\}_k$. However, individual transits from a periodic signal cannot be considered independent, and should instead be found periodically and share a common transit depth Δ. To this end, it can be shown (see Appendix B) that there is an analytical expression for the joint likelihood of K individual transits with depths and errors $\{\,\Delta_k, \sigma_k\,\}_k$ assuming a common depth Δ, corresponding to

$$\ln p(\boldsymbol{f}|P, T_0, D, \Delta) = \sum_k^K \ln \mathcal{L}_k - \frac{1}{2}\sum_k^K \left(\ln(\sigma_k^2) - \ln(\sigma^2 + \sigma_k^2) + \frac{(\Delta_k - \Delta)^2}{\sigma_k^2 + \sigma^2} \right)$$
$$\text{with} \quad \frac{1}{\sigma^2} = \sum_k^K \frac{1}{\sigma_k^2} \quad \text{and} \quad \Delta = \sigma^2 \sum_k^K \frac{\Delta_k}{\sigma_k^2}. \tag{7}$$

While Equation 7 takes a closed form, the individual epochs matching T_0 and P are not necessarily available in the grid of epochs $\{\,T_k\,\}_k$. In Foreman-Mackey et al. (2015), a similar issue is solved by using the nearest neighbors in the epochs grid. Instead, to allow the efficient matrix computation of Equation 7, the likelihood grid is linearly interpolated from $\{\,T_i\,\}_i$ to a common grid of transit phases $\{\,\phi_i\,\}_i$, leading to the periodic search log-likelihood

$$\ln \mathcal{P}(P) = \{\,\ln p(\boldsymbol{f}|P, \phi, D)\,\}_{i,j}$$

shown for few periods in Figure 5 (b). In the latter equation, $\Delta_{i,j}$ is omitted since being interpolated from the *linear search* using ϕ_i, D_j and $T_0 = 0$.

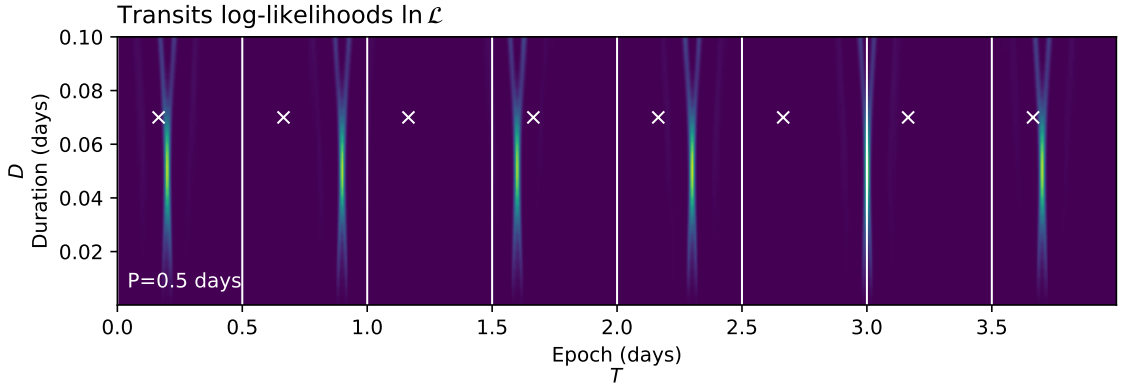

(a) $\ln \mathcal{L}$

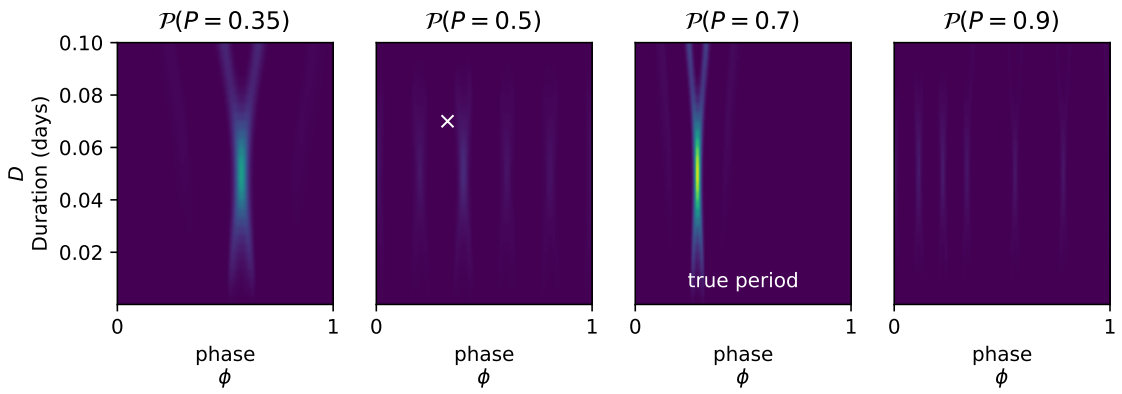

(b) $\mathcal{P}(P)$

Figure 5. Applied to the dataset shown Figure 4, this figure shows how the periodic search works at different periods P (including the true period $P = 0.7$ days). Given different periods P and $T_0 = 0$, the likelihood $\ln \mathcal{L}$ shown in (a) is phase-folded and interpolated onto a common grid of phases shown in (b). As an example, the white lines in (a) mark the edges of each fold for a period of $P = 0.5$ days, and the white crosses show the epochs $\{ T_k \}_{k \in \mathbb{K}}$ matching a particular phase in the grid (reported in (a) and (b)) on which the corresponding $\{ \ln \mathcal{L}_k \}_{k \in \mathbb{K}}$ are interpolated and combined using Equation 7. To allow the use of efficient matrix computations, this is done for all durations $\{ D_i \}_i$ so that $\mathcal{P}$ is computed on the full grid $\{ D_i, \phi_i \}_{i,j}$ at once. We understand from the folded likelihoods plots in (b) that a different choice of epoch T_0 may only shift the results in phase but do not affect the values of $\mathcal{P}$. For this reason, computing $\mathcal{P}$ for $T_0 = 0$ is sufficient. We also notice how the maximum value of $\mathcal{P}(P = 0.7/2)$ (left plot of (b)) is lower than for $P = 0.7$ days, a result of combining the log-likelihoods using Equation 7 instead of Equation 6, in favor of individual transits matching a common depth Δ.

2.3. *The transit search periodogram*

Using Equation 7, we can now compute $\ln \mathcal{P}$ for a range of periods and build a transit search periodogram using Equation 3. But a final issue emerges, one that is fundamentally linked to our strategy. Each likelihood $p(\boldsymbol{f}|T, D, \Delta)$ estimated during the *linear search* is computed using N measurements. Hence, combining transits in the periodic search, through Δ_k, σ_k and the product of K likelihoods $\{ \mathcal{L}_k \}_k$ (see Equation 7), artificially leads to a likelihood involving $N \times K$ measurements. This lead to a normalization issue when trying to compare the joint log-likelihoods $\mathcal{P}(P)$ from one period to another, as the number of observed transits differs from one period to another. This motivates a final step to produce the transit search periodogram $\mathcal{Q}$. For any period P, instead of taking $\mathcal{Q}(P)$ as the maximum value of $\ln \mathcal{P}$, the maximum likelihood parameters

$$(\phi_0, D) = \underset{\phi_i, D_j}{\arg\max} \{ \ln p(\boldsymbol{f}|P, \phi_i, D_j) \}_{i,j} \tag{8}$$

are retrieved, and $\mathcal{Q}(P)$ is defined as the SNR of the transit of period P, epoch $T_0 = \phi_0 P$, duration D and depth Δ, i.e.

$$\mathcal{Q}(P) = \frac{\Delta}{\sigma},$$

where Δ and σ are obtained using Equation B6 with the last column of X containing a periodic transit signal of period P, epoch T_0, duration D and depth 1. This process and the resulting periodogram $\mathcal{Q}$ are shown in Figure 6.

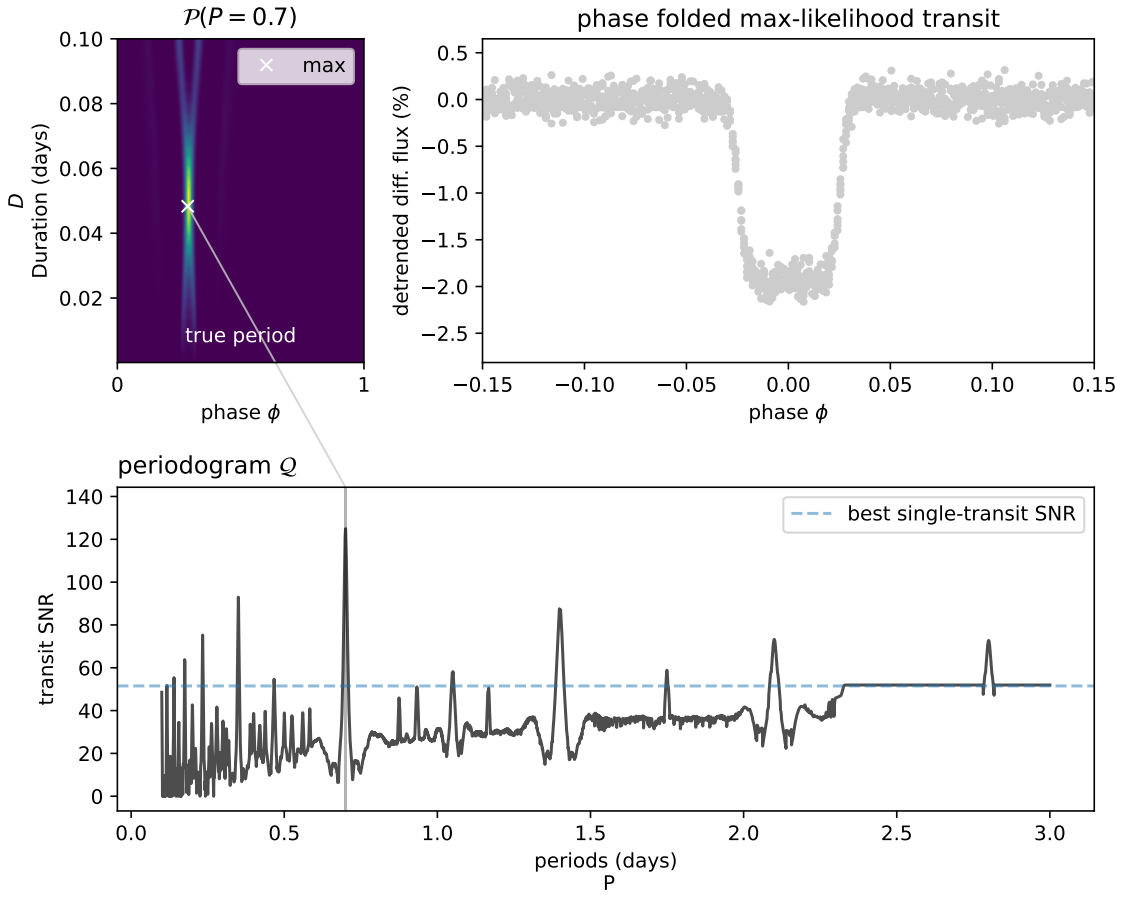

Figure 6. For each period P, the joint likelihood $\mathcal{P}(P)$ is computed using Equation 7, and the value of the maximum likelihood transit SNR retained as $\mathcal{Q}(P)$.

The periodic transit of period P with the maximum SNR, i.e. maximizing $\mathcal{Q}$, is adopted as the best candidate, basing the confidence in this signal through its SNR. The parameters of this transit are the period P, the epoch $T_0 = \phi_0 P$ and duration D (Equation 8), and the depth Δ with error σ (given by Equation B6).

2.4. *An open-source python package*

Methods presented in this paper are made accessible through the `nuance` open-source Python package, hosted on Github[5] and released on the Python Package Index (PyPI)[6].

[5] https://github.com/lgrcia/nuance
[6] https://pypi.org/project/nuance/

To instantiate a search, a user can start by creating a Nuance object with

```
from nuance import Nuance

nu = Nuance(time, flux, gp=gp, X=X)
```

where gp is a tinygp Gaussian Process instance and X the design matrix of the linear model. nuance exploits the use of tinygp[7], a Python package powered by JAX[8], allowing for custom kernels to be built and highly tractable computations. We can then define a set of epochs t0s and durations Ds and run the *linear search* with

```
import numpy as np

t0s = time.copy()
# a range of 10 durations
Ds = np.linspace(0.01, 0.2, 10)
nu.linear_search(t0s, Ds)
```

Finally, the periodic search is run with

```
# a wide range of periods
periods = np.linspace(0.1, 5, 2000)
search = nu.periodic_search(periods)
```

From this `search` object, the best transiting candidate parameters can be computed (search.best), or the $\mathcal{Q}$ periodogram retrieved (search.Q_snr), together with valuable information about the transit search. The Nuance object also provides methods to perform transit search on light curves from multi-planetary systems, the advantage of nuance being that the *linear search* only needs to be performed ones, and reused for the search of several transiting candidates. An extensive and maintained online documentation is provided at `nuance.readthedocs.io`.

2.5. *Comparison with BLS*

To start testing nuance against existing methods, a simple light curve is simulated, consisting in pure white noise with a standard deviation of 5×10^{-4} (relative flux), observed for a duration of 6 days with a cadence of 2 minutes. In this signal, box-shaped transits are injected with periods randomly sampled from 0.3 to 2.5 days, a unique transit duration of 50 minutes, and depths randomly sampled from 2.6×10^{-4} to 6.8×10^{-4} (using the simple model from Protopapas et al. (2005) presented in subsection A.1 with $c = 500$). By design, these injected signals have an SNR ranging from 5 to 30 (with $\sigma_r = 0$ in Equation 1). For each light curve, transits are searched using two different methods: nuance, using its implementation from the Python

[7] https://github.com/dfm/tinygp
[8] https://github.com/google/jax

package described in the previous section; and `BLS`, the box-least-square algorithm (Kovács et al. 2002), using the astropy BoxLeastSquares implementation[9]. For *nuance*

For both methods, 3000 trial periods from 0.2 to 2.6 days are searched, with a single trial duration fixed to the unique known duration of 50 minutes. A transit signal is considered detected if the absolute difference between the injected and the recovered period is less than 0.01 day. To ease the detection criteria, transit periods recovered at half or twice the injected period (aka *aliases*) are considered as being detected. For this reason, detected transit epochs are not considered. Results from this *injection-recovery* procedure are shown in Figure 7.

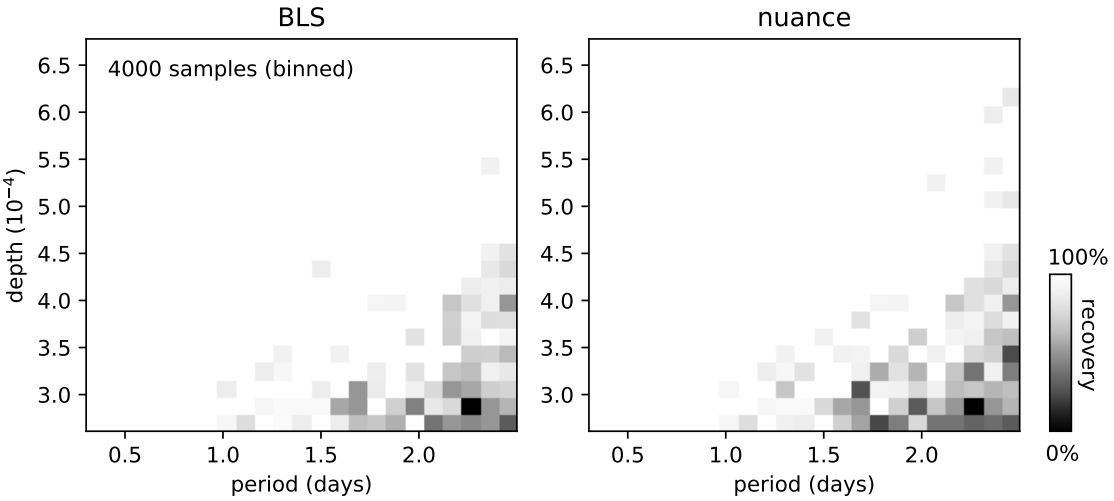

Figure 7. Binned statistics of the injection-recovery of 4000 transit signals in a flat light curve with only white noise (whose characteristics are described in the main text), using `BLS` and nuance. The color scale indicates the recovery of transits in the corresponding (period, depth) parameters space, white for a full recovery and black for no detection.

These results demonstrate the qualitative match between the detection capabilities of nuance and `BLS` on light curves with no correlated noise. Explaining the subtle differences observed between the two methods when only white noise is present is beyond the scope of this paper, and we will assume that any differences observed in the following sections are due to the different treatments of correlated noise.

[9] https://docs.astropy.org/en/stable/api/astropy.timeseries.BoxLeastSquares.html

3. RESULTS

3.1. *Comparison with* `biweight+BLS` *on simulated light curves*

Figure 3 shows that nuance's full-fledged modeling capabilities may not always be necessary and may only be beneficial for certain noise characteristics, relative to the searched transit parameters. Here, we evaluate the performance of nuance in the relative parameter space (τ, δ) described in Equation 2 and see when its specific treatment of correlated noise in the transit search becomes necessary.

We compare nuance to the approach that involves removing stellar variability from the light curves before performing the search on a detrended dataset. Similar to subsection 1.2, an optimal bi-weight filter implemented in the wõtan Python package[10] is used with a window size three times that of the injected transit duration. A transit search on the detrended light curve is then performed using the BLS algorithm, like in subsection 2.5 using the astropy BoxLeastSquares implementation[11]. This strategy is widely used in the community and is denoted `biweight+BLS`. In what follows, the transit detection criteria are the same as the ones used in subsection 2.5, i.e. that a transit is considered recovered if the absolute difference between the injected and recovered period is less than 0.01 days, including periods found at half or twice the injected ones (aliases) and ignoring the value of the recovered transit epoch.

DATASET

The dataset consists in 4000 light curves simulated using the model fully described in Appendix A. We simulate a common periodic transit added to all light curves, of period $P = 1.1$ days, epoch $T_0 = 0.2$ days, duration $D = 0.04$ days and depth $\Delta = 1\%$. Each light curve consists in a 4 days observation with an exposure time of 2 minutes, leading to $N = 2880$ data points with a normal error of 0.1%. As in subsection 2.5, only box-shaped transits are injected, using the model from Protopapas et al. (2005) with $c = 500$.

For a given pair of (τ, δ), we simulate stellar variability using a Gaussian Process with an SHO kernel of hyperparameters defined by Equation 2 (except for Q, described below), computed with respect to the injected transit parameters D and Δ. The same kernel is used for the search with nuance, an optimal choice on equal footing with the optimal $3 \times D$ window size of the bi-weight filter employed in the `biweight+BLS` search. While this kernel is optimal, a comprehensive discussion on the use of non-optimal kernels is discussed in . 4000 pairs of (τ, δ) are generated such that

$$\tau \sim \mathcal{U}(0.1, 10), \quad \delta \sim \mathcal{U}(0.1, 25) \quad \text{and} \quad Q \sim \mathcal{U}(10, 100)$$

where $\mathcal{U}(a, b)$ denotes a uniform distribution of lower bound a and upper bound b.

[10] https://github.com/hippke/wotan
[11] https://docs.astropy.org/en/stable/api/astropy.timeseries.BoxLeastSquares.html

The results of this injection-recovery procedure are shown in Figure 8 and highlight particularly well the benefit of `nuance` against the `biweight+BLS` strategy on transits with relatively low depth compared to the stellar variability amplitude, and a relatively small duration compared to the stellar variability period. This empirical statement only concerns light curves with a given amount of white noise, and may vary depending on the length of the observing window or the number of transits. For this reason, quantifying for which values of (τ, δ) `nuance` outperforms `biweight+BLS` would only apply to this specific example.

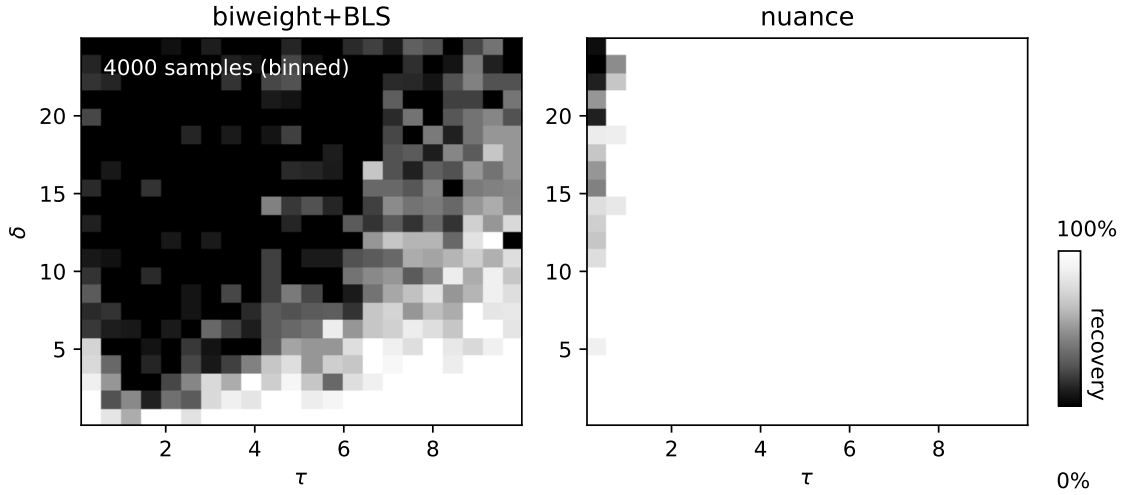

Figure 8. Injection-recovery results on 4000 simulated light curves described in section 3.1. The color scale represents the fraction of recovered transits, white if all injected transits are recovered in a given portion of the (τ, δ) parameter space, black if none are recovered.

This injection-recovery is done in a particularly optimal setup, on light curves not all physically realistic and using an optimal Gaussian Process kernel, hence demonstrating the performance of `nuance` only on a purely experimental basis. In the next section, we perform transits injection-recovery on real space-based light curves.

3.2. *Comparison with various techniques on limited TESS light curves*

In order to assess the performance of nuance on real datasets, we inject and recover transits into light curves from the Transiting Exoplanet Survey Satellite (TESS, Ricker et al. 2015). The goal of this transit injection-recovery is to compare nuance to other transit search strategies, and to understand the light curves characteristics for which it becomes beneficial.

We focus this proof of concept on light curves from a list of 438 M-dwarfs found to have detectable rotation signals with periods lower than one day (Ramsay et al. 2020), which lead to a parameter space justifying the use of *nuance*. For each of the studied target, transits are injected and recovered in the TESS 2 min cadence SPOC Simple Aperture Photometry and Pre-search Data Conditioning light curves (PDCSAP, Caldwell et al. 2020) of a single sector (the first being observed for each target) spanning on average 10 days.

In this injection-recovery tests, nuance is compared to other transit search strategies employing the `BLS` algorithm, for each of them after detrending the light curves with a different technique:

- `bspline+BLS` employs a B-spline[12] for detrending, fitted using the scipy.interpolate.splrep function[13], followed by a search with the `BLS` algorithm.
- `biweight+BLS` employs an optimal bi-weight filter implemented in the wõtan Python package (Hippke et al. 2019) with an optimal window size of $3 \times D$ (i.e. three times the transit duration), followed by a search with the `BLS` algorithm.
- `harmonics+BLS` employs a linear harmonic detrending, where the light curve is modeled as a Fourier series including four harmonics of the stellar rotation period found by Ramsay et al. (2020), with coefficients found through ordinary least square. This detrending is followed by a search with the `BLS` algorithm.
- `iterative+BLS` iteratively detrends the light curve with a sinusoidal signal fitted to the data, each time using the dominant period of the residuals found using a lomb-scargle periodogram (5 iterations). This detrending is followed by a search with the `BLS` algorithm.

LIGHT CURVE CLEANING AND TRANSITS INJECTION

As some of these techniques can be affected by gaps in the data, we only use continuous measurements from half a TESS sector. We assume that all methods (including

[12] https://docs.scipy.org/doc/scipy/reference/generated/scipy.interpolate.BSpline.html
[13] https://docs.scipy.org/doc/scipy/reference/generated/scipy.interpolate.splrep.html

nuance) are based on an incomplete model of the data that do not account for stellar flares. For this reason, the light curve of each target is cleaned using an iterative sigma clipping approach. For each iteration, points 3 times above the standard deviation of the full light curve (previously subtracted by its median) are identified. Then, the 30 adjacent points on each side of the found outliers are masked. This way, large flare signals and their expected ingress and egress are masked, using a total of 3 iterations. As PDCSAP light curves often start with a ramp-like signal, the first 300 points (as well as the last 300 points) of each continuous observation are masked. Finally, each light curve is normalized by its median value. Such a cleaned light curve is shown in Figure 9. We note that the gaps left after sigma clipping may be problematic for some of the detrending techniques (such as `bspline+BLS`). However, adopting this flare cleaning step and analyzing light curves with few small gaps is a practice commonly found in the literature.

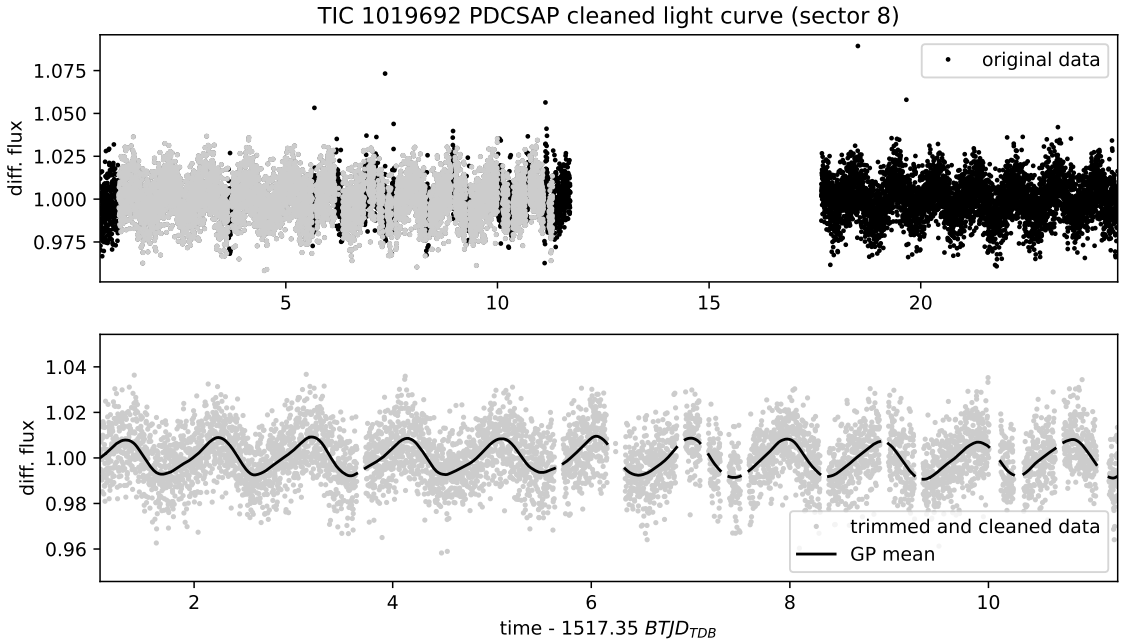

Figure 9. Trimmed and cleaned single-sector light curve of the target TIC 1019692. Top plot shows how much of the data is truncated and sigma clipped, resulting in a quasi-continuous light curve shown in the bottom plot. On this bottom plot, the black line corresponds to the mean of one of the Gaussian Process model (with hyperparameters optimized here on the cleaned light curve).

For each light curve, transits of planets with 10 different orbital periods combined with 10 planetary radii are individually considered, for a total of 100 periodic transits injections and recovery per target. Orbital periods P are sampled on a regular grid between 0.4 and 5 days, and planetary radii R_p are sampled on a regular grid designed to lead a minimum transit SNR of 4 and a maximum of 30. Using Equation 1 with

$\sigma_r = 0$, the planetary radius leading to a transit with a desired SNR s is given by

$$R_p = R_\star \, n^{-\frac{1}{4}} \sqrt{\sigma s}$$

with σ equal to the mean uncertainty estimated by the SPOC pipeline, $R_\star$ the radius of the star reported by Ramsay et al. (2020) and n the number of points in transit computed using a transit duration assuming a circular orbit.

STELLAR VARIABILITY KERNEL

One of the particularity of nuance is to model a light curve as a Gaussian Process. To model these TESS light curves, we employ a mixture of two SHO kernels of period $P_\star$ and $P_\star/2$ (with $P_\star$ the rotation period of the star), a model representative of a wide range of stochastic variability in stellar time series[14]. In order to account for additional corelated noises, we complement this kernel with a short and a long-timescale exponential term, so that the full kernel can be expressed as

$$k = k_1 + k_2 + k_3 + k_4$$

with

- k_1 a SHO kernel with hyperparameters

$$Q_1 = 1/2 + Q_0 + \delta Q\,, \quad \omega_1 = \frac{4\,\pi\,Q_1}{P\,\sqrt{4\,Q_1^2 - 1}} \quad \text{and} \quad S_1 = \frac{\sigma^2}{(1+f)\,\omega_1\,Q_1}.$$

- k_2 a SHO kernel with hyperparameters

$$Q_2 = 1/2 + Q_0\,, \quad \omega_2 = 2\omega_1 \quad \text{and} \quad S_2 = \frac{f\,\sigma^2}{(1+f)\,\omega_2\,Q_2},$$

where Q_0 is the quality factor for the secondary oscillation, δQ is the difference between the quality factors of the first and the second modes, f is the fractional amplitude of the secondary mode compared to the primary and σ is the standard deviation of the process. The kernels k_3 and k_4 are expressed as

$$k(t, t') = \sigma^2 \, \exp\left(-\frac{|t - t'|}{\ell}\right),$$

with ℓ and σ the scale and standard deviation of the process. These are meant to model short and long-timescale non-periodic correlated noise. In total, the rotation kernel k has 8 hyperparameters.

[14] https://celerite2.readthedocs.io/en/latest/api/python

The hyperparameters of this kernel are optimized on trimmed and cleaned light curves containing the injected transits, using the scipy.optimize.minimize[15] wrapper provided by the jaxopt Python package, and taking advantage of the JAX implementation of tinygp. As correlated noise is expected to affect the light curve uncertainty estimates performed by SPOC, the diagonal of the full covariance matrix of the data (i.e. their uncertainty, assuming homoscedasticity) is held free, increasing the number of optimized parameters to 9. The optimization is performed using the BFGS algorithm (Fletcher 1987), minimizing the negative log-likelihood of the data as expressed in Equation 4 (without transit), i.e. accounting for a linear systematic model of the data in addition of stellar variability. For simplicity, and to adopt a uniform treatment for all target light curves, a design matrix $\boldsymbol{X}$ with a single constant column is adopted, such that the systematic model only consists in a single parameter corresponding to the mean value of the differential flux (expected to be close to 1) solved linearly. The initial value for the rotation period of the star is found using a lomb-scargle periodogram (**??**) implemented in astropy[16].

SEARCH PARAMETERS AND TRANSIT DETECTION CRITERIA

For all techniques, we only search for transits with a duration fixed to the duration of the injected transits. This is mainly done for computational efficiency and allows for a narrower comparison between `nuance` and all `BLS`-based techniques. Finally, the search is done over 4000 trial periods linearly sampled from 0.3 to 6 days. Realistic transit searches on a wider parameter space (e.g. multiple trial durations) are discussed in **??**.

Like in previous sections, we consider the detection of period aliases and ignore the match between the injected and recovered transit epochs (although we visually vet that the found epochs were consistent with the ones injected for cases where the planet was detected). We consider a transit detectable if its original SNR is greater than 6. Hence we define *true positives* has detectable transits recovered with the correct period (or an alias) and a measured SNR greater or equal to 6, and *false positives* as non-detectable transits recovered with a measured SNR greater or equal to 6.

[15] https://jax.readthedocs.io/en/latest/_autosummary/jax.scipy.optimize.minimize.html
[16] https://docs.astropy.org/en/stable/timeseries/lombscargle.html

An example of the transit injection-recovery and its result is shown in Appendix C for the target TIC 1019692. Figure 11 shows the global results of the injection-recovery for all targets, while Figure 10 shows the true and false positives plotted against the relative parameters τ and δ (defined in). Compared to other methods, we find that `nuance` leads to the highest number of true positives, with a successful detection of 76% of the 7008 detectable transits injected (10950 with the non-dectable ones), and the lowest number of false negatives (Figure 11).

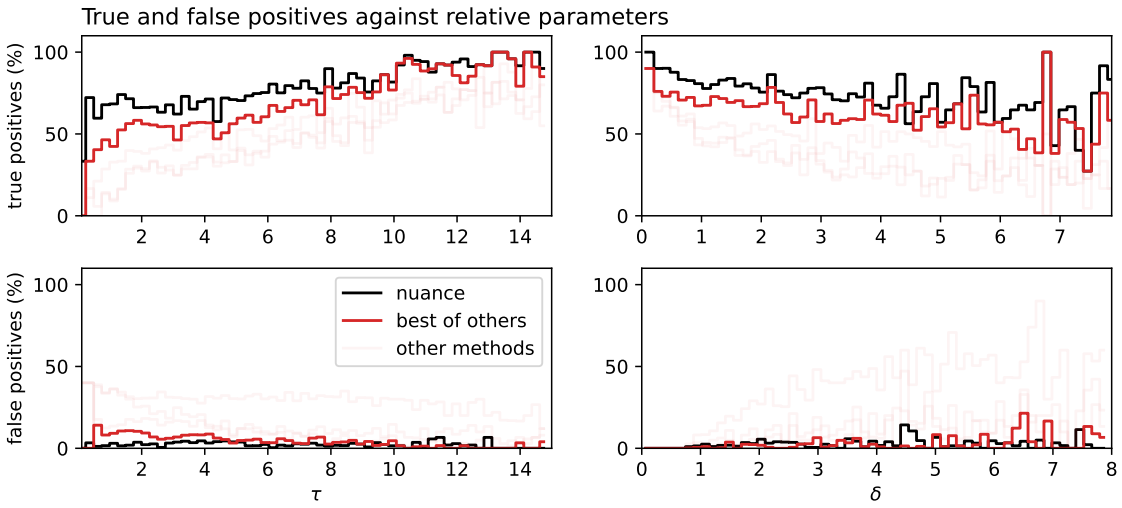

Figure 10. Rate of true and false positives of *nuance* compared to other methods, as a function of the relative parameters τ and δ. The solid red line corresponds to the maximum of true positives among all methods on the top panel, and the minimum of false positives on the bottom panel.

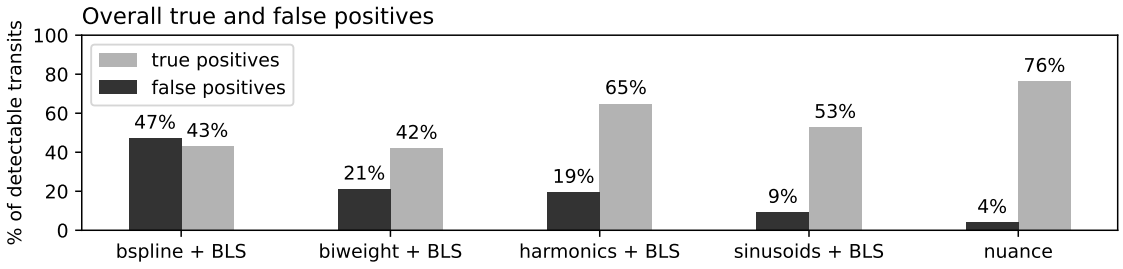

Figure 11. Rate of true and false positives for all methods as a fraction of detectable transit signals.

While the performances of other methods highly depend on the characteristics of the variability, *nuance* leads to the highest number of true positives in 79% of cases, and the lowest number of false positives in 72% of cases (Figure 10). When considering

both true and false positives simultaneously, *nuance* can be considered the best technique in only 55% of cases. However, **when considering transits with a relative timescale $\tau < 5$ (transits that justified the development of this algorithm), *nuance* is the best technique in 94% of cases, leading to both the highest number of true positives and the lowest number of false positives**.

3.3. *Comparison for a multi-sector TESS candidate: TOI-540*

In order to further validate nuance on a realistic dataset, we focus this section on the multi-sector TESS light curves of TOI-540, and the search for its earth-like companion TOI-540 b. We download the 2 min cadence SPOC PDCSAP light curves of TOI-540 observed in 5 sectors (4, 5, 6, 31 and 32). Like in the previous section, we use a Lomb-Scargle periodogram and identify the 0.72 days rotation period of the star, that we use as an initial value to optimize the kernel described in section 3.2 on each sector independently. Here again, we employ an upper-sigma-clipping to mask flares out of the data. The resulting light curve for sector 4 and its mean model is shown in Figure 12.

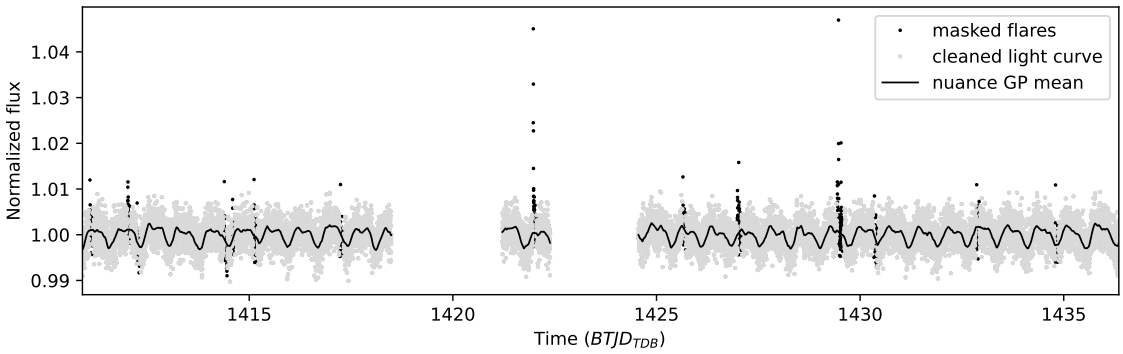

Figure 12. Sector 4 light curve of TOI 540. The clean signal (gray points) has been mask masked for flares (black points), and the black line corresponds to the mean of the Gaussian Process model.

For each sector, we perform the *linear search* of nuance on the cleaned light curve, using the original times as the trial epochs and 10 trial transit durations linearly sampled from 15 minutes to 1.5 hours. We then perform the periodic search on all sectors combined, using a concatenation of all linear searches. By adopting this by-sector GP modeling of the light-curve, the *linear search* of *nuance* scales linearly with the number of sectors being processed. This approach is adopted for efficiency but also to encapsulate the changing properties of stellar variability from one sector to another, often separated by year-long gaps. The periodic search is done on 20 000 trial periods ranging from 0.5 to 10 days. This search, using *nuance*, is compared to the more traditional approach that consists in detrending each sector with a bi-weight filter and then search for transits with the `BLS` algorithm (denoted `biweight+BLS` and described in subsection 3.2) on all sectors combined. Since we don't know the transit

duration a-priori, we employ a sliding window duration of 5 hours, small enough to encompass the stellar variability of TOI-540 but large enough not to detrend existing transits with durations lower tham 1.5 hours. The results of this comparison are shown in Figure 13.

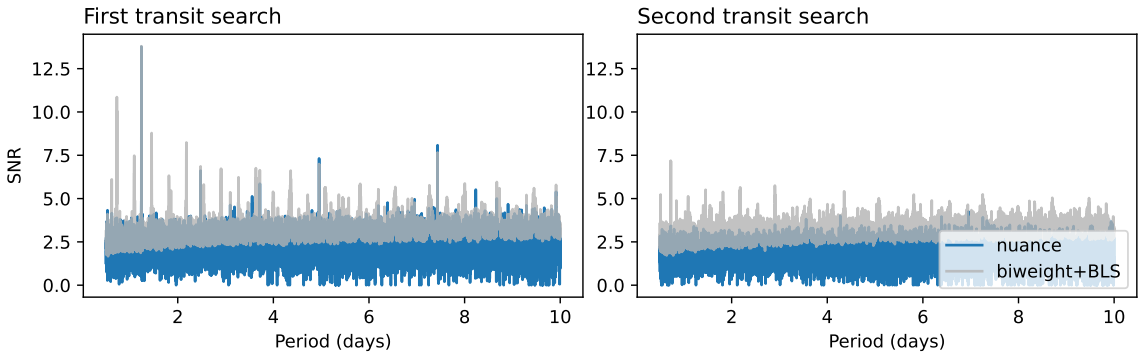

Figure 13. Transit search SNR periodograms of TOI-540 using `biweight+BLS` and *nuance*. After a first periodic search (left panel), the epochs corresponding to the maximum-SNR transit are masked before the second search is performed (right panel).

After a first periodic search, the times falling in the detected periodic transit signal (the one with an SNR higher than the detection limit set to 7) are masked. In practice, this is done by masking the linear search products

As seen in Figure 13, the SNR periodogram using `biweight+BLS` and `nuance` are very similar. This is well expected as the relative parameter τ equal 13 for TOI-540 b (using Equation 2 with the stellar rotation $P = 0.72$ days and the known transit duration $D = 29.5$ min of TOI-540 b (Ment et al. 2021)). Hence, as $\tau < 7$, the use of *nuance* on TOI-540 is not expected to be very beneficial (see Figure 3). Nonetheless, the *nuance* periodogram of TOI 540 features less spurious SNR peaks, largely due to the penalty naturally occurring when single transits with different depths are periodically combined. In the second search (right panel) of Figure 13, we also notice a higher number of peaks that would lead to false positive detections of transits in the `biweight+BLS` case. The proper treatment of correlated noise in *nuance*, as observed in subsection 3.2, makes these peaks non-significant, avoiding a large number of false detections.

We note that finding a TESS candidate that displays characteristics for which *nuance* is expected to be significantly beneficial proved to be very challenging during the writing of this paper, as transits with such characteristics are expected to be missed by current state-of-the-art techniques. We reserve the search for such new transit signals to a follow-up publication.

4. DISCUSSION

In the previous section we demonstrated the capability of *nuance* to search for synthetic or known transit signals, in simulated or real datasets. Here, we discuss the caveats of this algorithm, the advantages and limitations of the nuance implementation, and future prospects for its extension.

4.1. *Processing time*

In Figure 14, the processing time of nuance linear and periodic search are recorded against the number of points in a simulated light curve, assuming a simple non-optimized GP with a squared exponential kernel. These are compared to the processing time of `biweight+BLS` (cf. subsection 3.1) separated into the *biweight* filtering step and the BLS search.

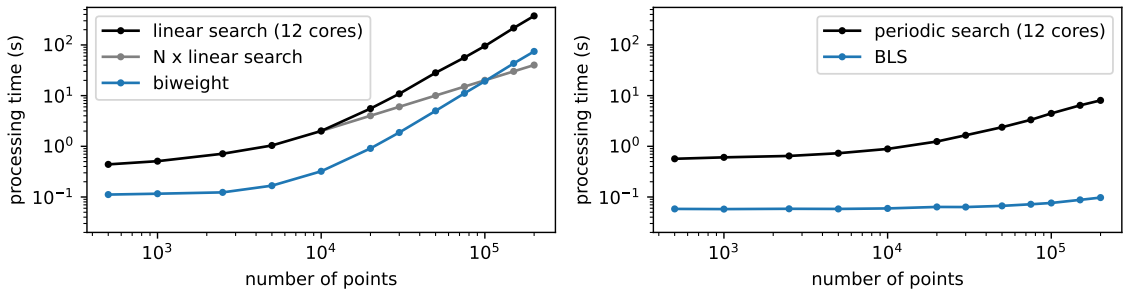

Figure 14. Study of nuance (black line) processing time against `biweight+BLS` (cf. subsection 3.1, blue line). The gray curve shows the performance of nuance *linear search* when applied to chunks of 10 000 points continuous observations, instead of considering these observations all together. This study is performed on both a single core of an Apple M2 Max chip (red line) and all of its 12 cores (black line). While not being shown, we verify that both the BLS algorithm and *nuance*processing times scale linearly with the number of probed transit durations and orbital periods.

As see in Figure 14, most of the computational cost of nuance and the `biweight+BLS` method comes from the *linear search* and the *biweight* filtering step. One advantage of *nuance* is that the *linear search* can be performed separately on different continuous observations, and then combined in the periodic search. Hence, if searching for transits in separate observations with approximately similar durations, such as different TESS sectors or different ground-based nightly observations, the computational cost of nuance grows linearly with the number of observations (see grey line in Figure 14). Nonetheless, considering a variety of other detrending algorithms, **nuance is expected to perform about one order of magnitude slower than more conventional techniques associated with BLS**. The second advantage of nuance is its JAX implementation, allowing the linear search to be run in parallel. As a reference, the 12 cores of an Apple M2 Max chip, searching for TOI-540 b transits with nuance (subsection 3.3) took 3 minutes in total, 1 minute for the 5 sectors linear searches, and 2 minutes for the combined periodic search. In comparison, the search with `biweight+BLS` took about 4 seconds.

Because of its computational cost, nuance must not be employed in the general case, but rather adopted when light curves contain correlated noise with specific characteristics. If employing a *biweight* filter for detrending, these characteristics correspond to the ones discussed in section 1. But as these strongly depend on the type of detrending technique employed, we do not provide general guidelines as when *nuance* should be preferred over a specific detrending technique. Nevertheless, extensive benchmarks and guidelines are reserved to future developments and will be progressively shared on nuance's online documentation[17].

4.2. *Systematics modeling*

Throughout the paper, a single column design matrix $\boldsymbol{X}$, corresponding to the mean differential flux (ideally unitary), was employed, hence assuming that the instrumental systematics signals were non-existent. In practice, *nuance* has been developed to linearly model systematic signals through more complex design matrices (as in Foreman-Mackey et al. 2015), in addition with its capability to model correlated noise while searching for transits. This feature is intentionally unexploited in the comparisons presented in section 3, as detrending light curves assuming a linear systematics model, such as PLD co-trending vectors (Deming et al. 2015), is highly incomplete if applied on data while ignoring the presence of other astrophysical signals. Comparisons involving more complex design matrices would also be sensitive to the choice of linear components, and would have unwanted repercussions on their results.

As an illustration, the NEMESIS pipeline (Feliz et al. 2021) starts processing the differential light curves by employing a linear systematics detrending using a least square fit of the data with a reduced PLD basis, before smoothing the signal from stellar variability using an approach similar to the one employed in the `biweight+BLS` approach (cf. subsection 3.2), hence detrending the systematics with an incomplete model that does not account for stellar variability. To account for stellar variability while fitting the linear systematics model to the data, a step further would be to use a GP, such as done in the EVEREST (Luger et al. 2018) pipeline. However this would also involve some potential degradation of the transit signals (see e.g. Figure 2), with a hardly distinguishable origin. For these reasons, and to keep our comparisons as targeted as possible, we do not compare commonly used systematics detrending approaches and decided to focus our study on the comparison with stellar variability detrending techniques (although these two aspects often overlap in the literature).

Although not being demonstrated here, modeling systematics signals while searching for transits on data acquired sparsly is extremely promising for the search of transit-

[17] https://nuance.readthedocs.io/en/latest/

ing exoplanets in ground-based data, that usually suffer from daily interruptions. In this respect, we note the similarity of our *linear search* (cf subsection 2.1) to the one presented in Berta et al. 2012, that focused on the detection of single eclipses in the MEarth light curves (Irwin et al. 2009). Similarly, ***nuance* would highly benefit the search for transiting exoplanets around M-dwarf type stars**, such as the ones observed by the SPECULOOS survey (Gillon 2018) whose monitoring suffers from both increased red noise (due to atmospheric and instrumental thermal effects discussed e.g. in Berta et al. 2012 and Pedersen et al. 2023) and enhanced stellar variability (Murray et al. 2020). We reserve this promising application to a future study.

4.3. *The choice of kernel*

While not being discussed in our study, the efficiency of *nuance* to detect transits in correlated noise is highly dependant on the design of its GP kernel. In the ensemble comparison of subsection 3.2, the goal was to choose a kernel and an optimization strategy suited to most of the studied light curves, leading to few outliers in the results that were indicative of a badly designed and/or optimized kernel. An alternative, recommended for more realistic blind searches, is to perform model comparison on well selected kernels, and to adapt the optimization strategy to each dataset.

When using nuance on TESS light curves for example, it must be noted that the observed light curve variability might originate from a contaminated photometric aperture, so that a physically-interpretable GP kernel representing a single star activity is not necessarily optimal.

5. CONCLUSION

We would like to thank Julien De Wit, Prajwal Niraula and Francisco J. Pozuelos for meaningful discussions at the beginning of this project, Germain Garcia for his useful insights about numerical optimization, Michaël Gillon for his overall support, and the member of the Astronomical Data Group at the Center for Computational Astrophysics for many enriching discussions and feedback.

APPENDIX

A. LIGHT CURVES SIMULATIONS

In order to study the effect of correlated noise on transit search, this paper relies on transit light curve simulations including realistic effects of stellar variability and instrumental signals. The following describes how such signals are modeled.

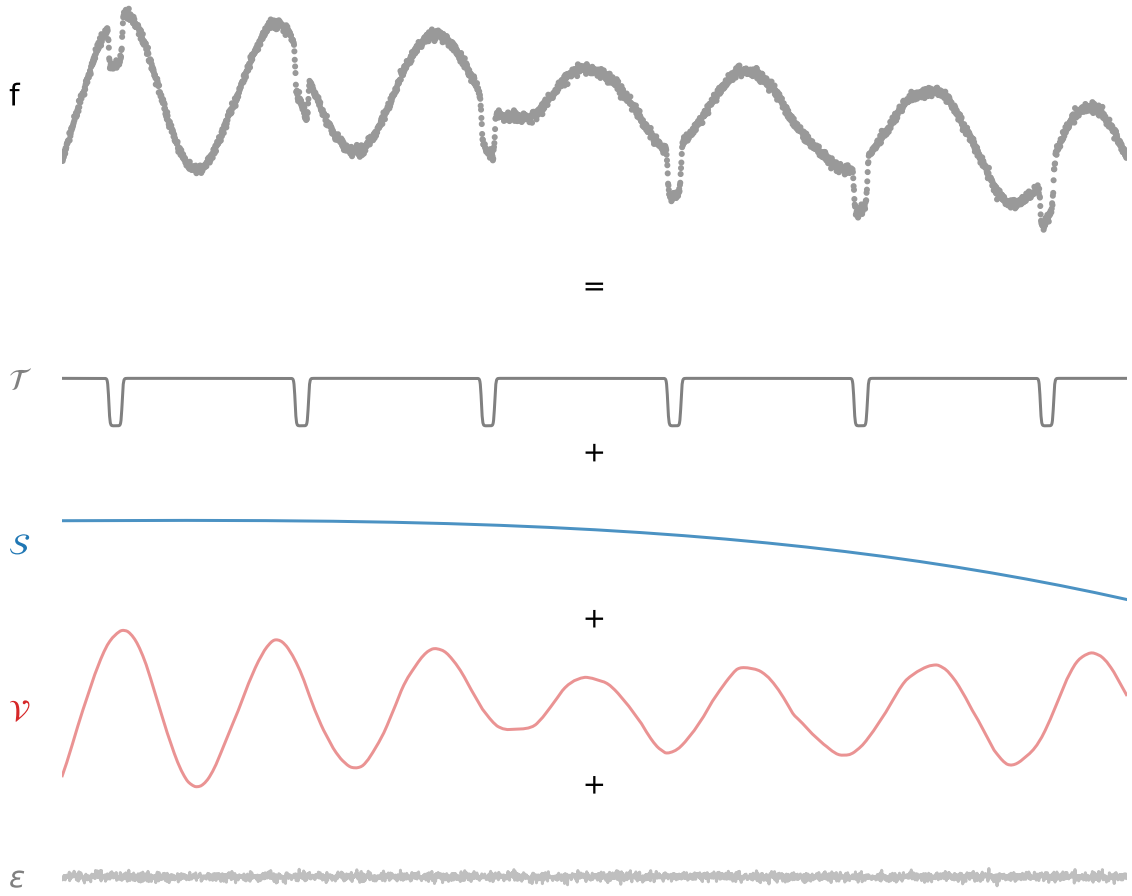

Figure 15. Example dataset sampled at $N = 2880$ times corresponding to an observation of 4 days with an exposure time of 2 minutes. The mean of this signal consists in a periodic transit signal of period $P = 0.7$ days, duration $D = 0.05$ days and depth of 2% ($\mathcal{T}$ in gray) plus instrumental signals ($\mathcal{S}$ in blue). Correlated noise in the form of stellar variability is simulated by modeling the covariance matrix of the signal with a Gaussian process ($\mathcal{V}$ in red) including a diagonal variance of 0.001^2 corresponding to white noise (ϵ in light grey). This simulated signal is not intended to be physically realistic.

Let f be the simulated flux of a star sampled and arranged in the vector $\boldsymbol{f}$ associated to the vector of times $\boldsymbol{t}$, such that

$$\boldsymbol{f} \sim \mathcal{N}(\boldsymbol{\mu}, \boldsymbol{C}),$$

i.e. that $\boldsymbol{f}$ is drawn from a Gaussian process of mean $\boldsymbol{\mu}$ and covariance matrix $\boldsymbol{C}$. In this equation, $\boldsymbol{\mu}$ is such that its i-th element is defined by $\mu_i = \mathcal{T}(t_i) + \mathcal{S}(t_i)$ where t_i is the i-th time of observation, $\mathcal{T}$ is a periodic transit function and $\mathcal{S}$ a function describing the instrumental part of the signal (both described below). The covariance matrix $\boldsymbol{C}$ is built such that $C_{i,j} = k(t_i, t_j)$ where k is a covariance function (or *kernel*) accounting for correlated noise in the form of stellar variability (with added white noise). An example of such signal is simulated and shown in Figure 15.

A.1. *Transit signal* $\mathcal{T}$

The periodic transit signal $\mathcal{T}$ is simulated using the simple model described in Protopapas et al. (2005), where a transit of period P, epoch T_0, duration D and unitary depth observed at time t is given by

$$\begin{aligned} \mathcal{T}_c(t, P, T_0, D) &= \frac{1}{2}\tanh\left(c\left[\theta - \frac{1}{2}\right]\right) - \frac{1}{2}\tanh\left(c\left[\theta + \frac{1}{2}\right]\right), \\ \text{with} \quad \theta &= \frac{P}{\pi D}\sin\left(\frac{\pi(t - T_0)}{P}\right), \end{aligned} \tag{A1}$$

where the dimensionless parameter c controls the roundness of the transit depth ($c \gg 1$ corresponding to a box-shaped transit as shown in Figure 16). This analytical model is fully empirical but easily differentiable.

Figure 16. Simulations of a single transit signal (Equation A1) shown for different values of c.

In this paper, unless specified, all transits are simulated with $c = 12$, a value arbitrarily chosen that can be fined-tuned in real applications using the limb-darkening coefficients of a given star. The periodic transit signal $\mathcal{T}$ seen in Figure 15 corresponds to $\mathcal{T} = 0.02 \times \mathcal{T}_{c=12}(\boldsymbol{t}, P = 0.7, T_0 = 0.2, D = 0.05)$, all parameters in unit of days.

A.2. *Instrumental signals* $\mathcal{S}$

Instrumental signals are simulated as a linear model of M explanatory variables arranged in the $(N \times M)$ design matrix $\boldsymbol{X}$. Hence,

$$\mathcal{S} = \boldsymbol{X}\boldsymbol{w},$$

where the vector $\boldsymbol{w}$ contains the linear coefficients of the model. The simulated flux shown in Figure 15 contains a linear model where the $M = 4$ columns of the design matrix $\boldsymbol{X}$ are given by $\boldsymbol{X}_i = \boldsymbol{t}^i$ (i.e. $\boldsymbol{X}$ is the Vandermonde matrix order 3 of time t) and $\boldsymbol{w} = [1.0 \quad 0.0005 \quad -0.0002 \quad -0.0005]$.

A.3. *Stellar variability* ν

As this chapter focuses on stellar variability and its effect on transit detection, We employ a simple physically-motivated Gaussian Process kernel, describing stellar variability through the covariance of a stochastically-driven damped harmonic oscillator (SHO, Foreman-Mackey et al. 2017; Foreman-Mackey 2018) taking the form

$$k(\tau) = \sigma^2 \exp\left(-\frac{\omega\,\tau}{2\,Q}\right) \begin{cases} 1 + \omega\,\tau & \text{for } Q = 1/2 \\ \cosh(f\,\omega\,\tau/2\,Q) + \sinh(f\,\omega\,\tau/2\,Q)/f & \text{for } Q < 1/2 \\ \cos(g\,\omega\,\tau/2\,Q) + \sin(g\,\omega\,\tau/2\,Q)/g & \text{for } Q > 1/2 \end{cases} \tag{A2}$$
$$\text{where} \quad \tau = |t_i - t_j|, \quad f = \sqrt{1 - 4\,Q^2} \quad \text{and} \quad g = \sqrt{4\,Q^2 - 1}$$

where Q is the quality factor of the oscillator, ω its pulsation and σ the amplitude of the kernel function. Gaussian Process computations in this paper use the implementation from `tinygp`[18], a Python package exposing the quasi-separable kernels from Foreman-Mackey (2018) and powered by `JAX`[19]. The stellar variability signal in Figure 15 has been sampled from a Gaussian Process with an SHO kernel of parameters $\omega = \pi/6D$ (i.e. a period equal to 12 times the duration D of the simulated transit), $Q = 45$ and $\sigma = 0.02$, the depth of the simulated transit. An extra term $\sigma_f^2 = 0.001^2$ is added to the diagonal of the covariance matrix, corresponding to the variance of the simulated measurement f and leading to the white noise observed in Figure 15.

B. PROOF FOR THE PERIODIC SEARCH EXPRESSION

From the *linear search* presented in subsection 2.1, we retain and index by k the parameters of the K individual transits whose epochs $\{T_k\}_k$ are compatible with a periodic signal of period P and epoch T_0. From the likelihoods of these transits (computed in subsection 2.1), we want an expression for

$$p(\boldsymbol{f}|P, T_0, D, \Delta) = \prod_{k \in \mathbb{T}} p(\boldsymbol{f}|T_k, D, \Delta),$$

i.e., given a depth D, the likelihood of the data given a periodic transit signal of period P, epoch T_0 and a common depth Δ. Since only $\{p(\boldsymbol{f}|T_k, D, \Delta_k)\}_k$ is known (i.e. transits with different depths), we decompose

$$p(\boldsymbol{f}|T_k, D, \Delta) = \int p(\boldsymbol{f}|T_k, D, \tilde{\Delta}) p(\tilde{\Delta}|\Delta)\, d\tilde{\Delta}, \tag{B3}$$

where $p(\boldsymbol{f}|T_k, D, \tilde{\Delta})$ is the probability of the k-th transit to have a depth $\tilde{\Delta}$ and $p(\tilde{\Delta}|\Delta)$ the probability to observe the depth $\tilde{\Delta}$ knowing the existence of a common depth Δ. In other words, Equation B3 involves the likelihood of the non-periodic transit k to be part of a periodic transit signal with a common depth Δ.

[18] https://github.com/dfm/tinygp
[19] https://github.com/google/jax

Since each depth Δ_k is found through generalized least square, each follow a normal distribution $\mathcal{N}(\Delta_k, \sigma_k^2)$, centered on Δ_k with variance σ_k^2 and an amplitude $\mathcal{L}_k$, leading to the likelihood function

$$p(\boldsymbol{f}|T_k, D, \tilde{\Delta}) = \mathcal{L}_k \exp\left(-\frac{(\tilde{\Delta} - \Delta_k)^2}{2\sigma_k^2}\right).$$

As for the common transit depth Δ, it can be estimated through the joint probability of all other transit depths than Δ_k, such that

$$\Delta \sim \prod_{i \neq k}^{K} \mathcal{N}(\Delta_i, \sigma_i^2),$$

with

$$\frac{1}{\sigma^2} = \sum_{i \neq k}^{K} \frac{1}{\sigma_i^2} \quad \text{and} \quad \Delta = \sigma^2 \sum_{i \neq k}^{K} \frac{\Delta_i}{\sigma_i^2}. \tag{B4}$$

Hence

$$p(\tilde{\Delta}|\Delta) = \frac{1}{\sqrt{2\pi\sigma^2}} \exp\left(-\frac{(\tilde{\Delta} - \Delta)^2}{2\sigma^2}\right).$$

We can now rewrite Equation B3 as

$$p(\boldsymbol{f}|T_k, D, \Delta) = \frac{\mathcal{L}_k}{\sqrt{2\pi\sigma^2}} \int \exp\left(-\frac{(\tilde{\Delta} - \Delta_k)^2}{2\sigma_k^2}\right) \exp\left(-\frac{(\tilde{\Delta} - \Delta)^2}{2\sigma^2}\right) d\tilde{\Delta}.$$

The integral in this equation is a product of gaussian integrals that can be obtained analytically, leading to

$$p(\boldsymbol{f}|T_k, D, \Delta) = \mathcal{L}_k \sqrt{\frac{\sigma_k^2}{\sigma^2 + \sigma_k^2}} \exp\left(-\frac{1}{2}\frac{(\Delta_k - \Delta)^2}{\sigma_k^2 + \sigma^2}\right).$$

Finally,

$$\ln p(\boldsymbol{f}|P, T_0, D, \Delta) = \sum_{k}^{K} \ln \mathcal{L}_k - \frac{1}{2} \sum_{k}^{K} \left(\ln(\sigma_k^2) - \ln(\sigma^2 + \sigma_k^2) + \frac{(\Delta_k - \Delta)^2}{\sigma_k^2 + \sigma^2}\right), \tag{B5}$$

the log-likelihood of the data given a periodic transit signal of period P, epoch T_0, duration D and common depth Δ. In order to reduce the number of times Equation B4 is computed, we adopt the biased estimates

$$\frac{1}{\sigma^2} = \sum_{k}^{K} \frac{1}{\sigma_i^2} \quad \text{and} \quad \Delta = \sigma^2 \sum_{k}^{K} \frac{\Delta_i}{\sigma_i^2}, \tag{B6}$$

so that Δ and σ are independent of k in the last sum of Equation 7.

C. INJECTION-RECOVERY ON TIC 1019692

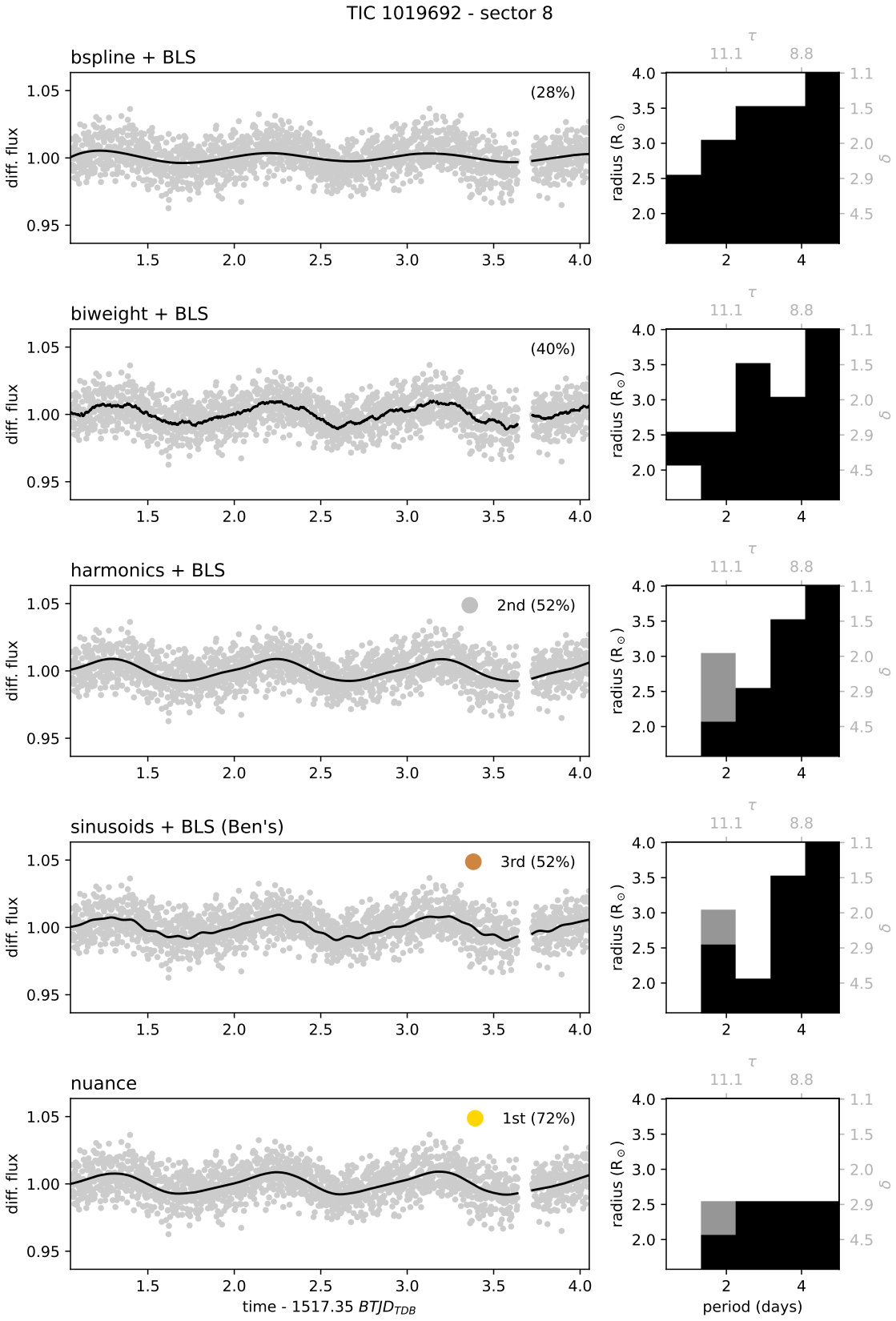

Figure 17. Results of the transits injection-recovery on TIC 1019692 half-sector light curve. Left: cleaned light curve with computed trend overplotted in black (except for nuance where it corresponds to the mean of the Gaussian Process model). Right: Results of the transit search where a black square denotes a transit signal not detected, gray a signal detected at an alias period ($P/2$ or $2P$), and white a signal detected with the correct period. On the right plots, secondary axes show the (τ, δ) relative parameter space. For each method, the upper right legend on the left plot indicates its ranking based on the percent of recovered transit signals (where a transit with an aliased period counts as being detected).

REFERENCES

Aigrain, S., Parviainen, H., & Pope, B. J. S. 2016, MNRAS, 459, 2408, doi: 10.1093/mnras/stw706

Berta, Z. K., Irwin, J., Charbonneau, D., Burke, C. J., & Falco, E. E. 2012, AJ, 144, 145, doi: 10.1088/0004-6256/144/5/145

Caldwell, D. A., Tenenbaum, P., Twicken, J. D., et al. 2020, Research Notes of the American Astronomical Society, 4, 201, doi: 10.3847/2515-5172/abc9b3

Deming, D., Knutson, H., Kammer, J., et al. 2015, ApJ, 805, 132, doi: 10.1088/0004-637X/805/2/132

Feliz, D. L., Plavchan, P., Bianco, S. N., et al. 2021, AJ, 161, 247, doi: 10.3847/1538-3881/abedb3

Fletcher, R. 1987, Practical methods of optimization: V. 1-2, 2nd edn. (Chichester, England: John Wiley & Sons)

Foreman-Mackey, D. 2018, Research Notes of the American Astronomical Society, 2, 31, doi: 10.3847/2515-5172/aaaf6c

Foreman-Mackey, D., Agol, E., Ambikasaran, S., & Angus, R. 2017, AJ, 154, 220, doi: 10.3847/1538-3881/aa9332

Foreman-Mackey, D., Montet, B. T., Hogg, D. W., et al. 2015, ApJ, 806, 215, doi: 10.1088/0004-637X/806/2/215

Gillon, M. 2018, Nature Astronomy, 2, 344, doi: 10.1038/s41550-018-0443-y

Hippke, M., David, T. J., Mulders, G. D., & Heller, R. 2019, AJ, 158, 143, doi: 10.3847/1538-3881/ab3984

Howell, S. B., Ciardi, D. R., Giampapa, M. S., et al. 2016, AJ, 151, 43, doi: 10.3847/0004-6256/151/2/43

Irwin, J., Charbonneau, D., Nutzman, P., & Falco, E. 2009, in Transiting Planets, ed. F. Pont, D. Sasselov, & M. J. Holman, Vol. 253, 37–43, doi: 10.1017/S1743921308026215

Jenkins, J. M., Chandrasekaran, H., McCauliff, S. D., et al. 2010, in Society of Photo-Optical Instrumentation Engineers (SPIE) Conference Series, Vol. 7740, Software and Cyberinfrastructure for Astronomy, ed. N. M. Radziwill & A. Bridger, 77400D, doi: 10.1117/12.856764

Kovács, G., Bakos, G., & Noyes, R. W. 2005, MNRAS, 356, 557, doi: 10.1111/j.1365-2966.2004.08479.x

Kovács, G., Hartman, J. D., & Bakos, G. Á. 2016, A&A, 585, A57, doi: 10.1051/0004-6361/201527124

Kovács, G., Zucker, S., & Mazeh, T. 2002, A&A, 391, 369, doi: 10.1051/0004-6361:2002080210.48550/arXiv.astro-ph/0206099

Luger, R., Agol, E., Kruse, E., et al. 2016, AJ, 152, 100, doi: 10.3847/0004-6256/152/4/100

Luger, R., Kruse, E., Foreman-Mackey, D., Agol, E., & Saunders, N. 2018, AJ, 156, 99, doi: 10.3847/1538-3881/aad230

Ment, K., Irwin, J., Charbonneau, D., et al. 2021, AJ, 161, 23, doi: 10.3847/1538-3881/abbd91

Morris, B. M., Hebb, L., Davenport, J. R. A., Rohn, G., & Hawley, S. L. 2017, ApJ, 846, 99, doi: 10.3847/1538-4357/aa8555

Mosteller, F., & Tukey, J. W. 1977, Data analysis and regression. A second course in statistics

Murray, C. A., Delrez, L., Pedersen, P. P., et al. 2020, MNRAS, 495, 2446, doi: 10.1093/mnras/staa1283

Newton, E. R., Rampalli, R., Kraus, A. L., et al. 2022, AJ, 164, 115, doi: 10.3847/1538-3881/ac8154

Pedersen, P. P., Murray, C. A., Queloz, D., et al. 2023, MNRAS, 518, 2661, doi: 10.1093/mnras/stac3154

Pont, F., Zucker, S., & Queloz, D. 2006, MNRAS, 373, 231, doi: 10.1111/j.1365-2966.2006.11012.x

Protopapas, P., Jimenez, R., & Alcock, C. 2005, MNRAS, 362, 460, doi: 10.1111/j.1365-2966.2005.09305.x

Rackham, B. V., Apai, D., & Giampapa, M. S. 2018, ApJ, 853, 122, doi: 10.3847/1538-4357/aaa08c

Ramsay, G., Doyle, J. G., & Doyle, L. 2020, MNRAS, 497, 2320, doi: 10.1093/mnras/staa2021

Rasmussen, C. E., & Williams, C. K. I. 2005, Gaussian processes for machine learning, Adaptive Computation and Machine Learning series (London, England: MIT Press)

Ricker, G. R., Winn, J. N., Vanderspek, R., et al. 2015, Journal of Astronomical Telescopes, Instruments, and Systems, 1, 014003, doi: 10.1117/1.JATIS.1.1.014003

Simpson, E. R., Fetherolf, T., Kane, S. R., et al. 2023, AJ, 166, 72, doi: 10.3847/1538-3881/acda26

Skumanich, A. 1972, ApJ, 171, 565, doi: 10.1086/151310

Tamuz, O., Mazeh, T., & Zucker, S. 2005, MNRAS, 356, 1466, doi: 10.1111/j.1365-2966.2004.08585.x